Langmuir

Article

pubs.acs.org/Langmuir

Binding Geometry of Hydrogen-Bonded Chain Motif in Self-Assembled Gratings and Layers on Ag(111)

J. Lipton-Duffin,[†,◆] J.A. Miwa,[†,◆] S. G. Urquhart,[‡] G. Contini,[§,∥] A. Cossaro,[⊥] L. Casalis,[#] J. V. Barth,[○] L. Floreano,[⊥] A. Morgante,[⊥,#,▽] and F. Rosei*[,†]

[†]Centre Énergie, Matériaux et Télécommunications, Institut National de la Recherche Scientifique, Université du Québec, 1650 Boulevard Lionel-Boulet, Varennes, QC, J3X 1S2, Canada

[‡]Department of Chemistry, University of Saskatchewan, 110 Science Place, Saskatoon, SK S7N 5C9, Canada

[§]Istituto di Struttura della Materia, CNR, Via Fosso del Cavaliere 100, 00133 Roma, Italy

[∥]Centro interdipartimentale Nanoscienze & Nanotecnologie & Strumentazione (NAST), University of Rome "Tor Vergata", 00133 Roma, Italy

[⊥]CNR-IOM, Laboratorio TASC, Trieste, 34149 TS, Italy

[#]Sincrotrone Trieste S.C.p.A., 34149 Trieste, Italy

[▽]Department of Physics, University of Trieste, I-34127 Trieste, Italy

[○]Physik Department, Technische Universität München, James-Franck Straße, 185748 Garching, Germany

Supporting Information

ABSTRACT: Upon adsorption on the (111) facet of Ag, 4-[*trans*-2-(pyrid-4-yl-vinyl)] benzoic acid (PVBA) self-assembles into a highly ordered, chiral twin chain structure at submonolayer coverages with domains that can extend for micrometers in one dimension. Using polarization-dependent measurements of C and N K-shell excitations in near-edge X-ray absorption fine structure (NEXAFS) spectra, we determine the binding geometry of single PVBA molecules within this unique ensemble for both low and high coverage regimes. At submonolayer coverage, the molecule is twisted to facilitate the formation of hydrogen bonds. The gas-phase planarity is gradually recovered as the coverage is increased, with complete planarity coinciding with loss of order in the overlayer. Thermal treatment of the PVBA film results in deprotonation of the carboxyl tail of the molecule, but despite the suppression of the stabilizing hydrogen-bonds, the overlayer remains ordered.

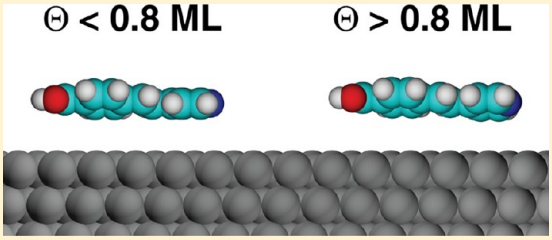

INTRODUCTION

The self-assembly of organic molecules on surfaces via noncovalent interactions typically is driven by combinations of van der Waals forces, hydrogen bonding, or metal−organic coordination.[1−18] Much effort has been directed at understanding both the fundamental static and dynamic processes at the molecular level, as well as at optimizing the growth of thin films for use as active materials in, for example, organic electronic devices,[17,19−23] biosensors[24] or liquid crystal displays.[25] In the context of these applications, it is desirable to probe the degree of orientation of the functional layers to predict their properties, as well as their capability to underpin further growth beyond single two-dimensional (2D) layers. Revealing the structural details of organic/inorganic interfaces with molecular precision offers a pathway to developing organic electronic devices with tailored and optimized features. Important properties of organic molecules that influence device performance (such as charge carrier mobility, absorption and luminescence) are, in general, highly anisotropic,[22,23,26−29] and will thus strongly depend on the orientation of the molecules with respect to one another and the supporting substrate.

The aromatic molecule 4-[*trans*-2-(pyrid-4-yl-vinyl)]benzoic acid (PVBA) was originally synthesized for use in nonlinear optics applications.[30,31] Except for a few reports regarding the nonlinear optical properties of PVBA thin films,[30−32] studies of PVBA hitherto have provided fundamental insights into surface self-assembly and chirality.[12,13,33−39]

In the gas phase PVBA is achiral, but following 2D confinement when adsorbed on a surface, two conformers can exist.[40] The two possible orientations of the carboxylic acid group are disregarded since it has been established that the hydrogen atom may move freely between the two oxygen atoms when similar molecules are adsorbed on a surface.[40] On the (111) facet of Ag, PVBA segregates into homochiral domains that can extend up to lengths of micrometers.[35,40]

The scanning tunneling microscope (STM) image presented in Figure 1a shows that the molecules line up head-to-tail into coupled chains that are oriented parallel to the $\langle 11\bar{2} \rangle$ direction.

Received: July 25, 2012
Revised: September 10, 2012
Published: September 12, 2012

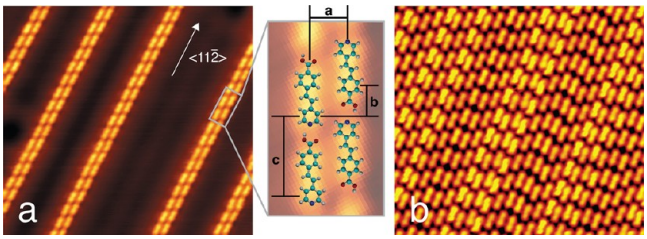

Figure 1. (a) (9 × 17 nm^2) A high-resolution STM image of the PVBA ($C_{13}NH_{10}COOH$) chiral twin chains reveals the internal structure of the twin chains. Each chain consists of coupled PVBA molecules, as shown on the zoomed inset. (b) (24 × 24 nm^2) At higher coverages the pairing between adjacent chains is disrupted, and some molecules appear brighter, suggesting a new adsorption geometry. Images adapted from refs 34 and 40.

This arrangement reflects appreciable hydrogen bonding between pyridyl and carboxylic acid end groups. Coupled chain pairs within a particular domain have lateral separation distances ranging from 2.5 to 5.0 nm; the distance between the chain pairs can be modulated by adjusting the PVBA surface coverage.[40] The coupling between adjacent chains is thought to be driven by weak lateral attractive interactions between the carbonyl and pyridyl moieties of neighboring PVBA molecules (O1···H2, see Figure 6). Adjacent chains are spaced by 0.69 nm (distance 'a' in the zoomed inset of Figure 1) and longitudinally displaced with respect to one another along the chain direction by 0.37 nm (distance 'b'); the chain stride is 1.5 nm (distance 'c'), and PVBA molecules within a chain are coupled together via hydrogen bonding in a head-to-tail arrangement.[35,40] Notably, the domains are enantiopure, and the chains themselves are chiral since the chains that compose a pair are displaced with respect to one another. The chiral twin chains thus arise due to the prochiral nature of PVBA, their adsorption geometry, and the head-to-tail hydrogen bonding between PVBA molecules.[33,40,41] At coverages above 0.8 ML, the pairing between the chains is disrupted, and certain PVBA building blocks appear brighter than others, as seen in Figure 1b. This behavior may suggest an alternate adsorption geometry at coverages beyond the first monolayer, and points to the exciting possibility of nanoscale patterning of additional molecular layers toward controlled three-dimensional (3D) structuring from the bottom-up.[42]

The adsorption of PVBA on Ag,[35,38,40,41] Au,[34] and other metal surfaces such as Cu[43,44] and Pd[36,37,45] is well documented. However, questions regarding the molecular conformation remain unanswered; in particular, do the phenyl and pyridyl end groups of PVBA molecules within the chain structure lie flat on the surface, as suggested by STM observations, or does the molecule retain its gas-phase planarity, but adsorb with an overall tilt with respect to the surface? Or, does the flexibility of PVBA combined with directional hydrogen bonding between molecules within the chain structure induce conformational distortions, such as an out-of-plane rotation of the head and tail moieties, as observed in other similar flexible molecules?[46−48]

In this paper, we report a detailed investigation of the adsorption of PVBA on Ag(111) by near-edge X-ray absorption fine structure (NEXAFS). We show that PVBA adopts a twisted geometry when participating in the twin-line structure, at coverages below Θ = 0.8 ML. The twist is relaxed as the coverage is increased, recovering its gas-phase planar conformation at multilayer coverage on the Ag(111) surface, but with an overall tilt angle of approximately 24 ± 3° between the plane of the aromatic rings and the surface normal. The reduced twist of the molecule goes hand-in-hand with the weakening of the hydrogen-bond responsible for the paired geometry observed in the chains at lower coverages, and explains the loss of these pairs beyond the threshold coverage.

METHODS

The experiments were performed at the ALOISA beamline of the ELETTRA Synchrotron Light Source in Trieste, Italy. The ALOISA beamline is equipped with an undulator source that provides linearly polarized X-rays, and hosts an end-station consisting of two ultrahigh vacuum (UHV) chambers for preparation and analysis, both with a base pressure in the low 10^{-10} mbar range. The preparation of the PVBA dosed surface was performed in situ. A single crystal of Ag(111) was cleaned by repeated cycles of 0.5−2.0 keV Ar^+ sputtering and annealing to 825−840 K. The cleanliness of the sample was subsequently verified by X-ray photoelectron spectroscopy (XPS). After several hours of degassing at 430 K, PVBA was sublimated from a Knudsen-cell-type evaporator at a temperature of 425 K onto a Ag(111) surface held at 300 K. The XPS intensity ratio of the C 1s to Ag 3d core levels was used as a measure of the coverage (see Supporting Information); the appearance in the reflection high energy electron diffraction (RHEED) pattern of additional symmetry spots in the $\langle 01\bar{1}\rangle$ azimuthal incidence directions confirmed the formation of twinned chains (see Supporting Information). The sample was then cooled to about 180 K to reduce possible molecular decomposition under X-ray irradiation and improve the energy resolution; this temperature was maintained throughout the spectroscopic measurements.

The NEXAFS C and N K-edge spectra were recorded, using the experimental geometry illustrated in Figure 2 with photon grazing

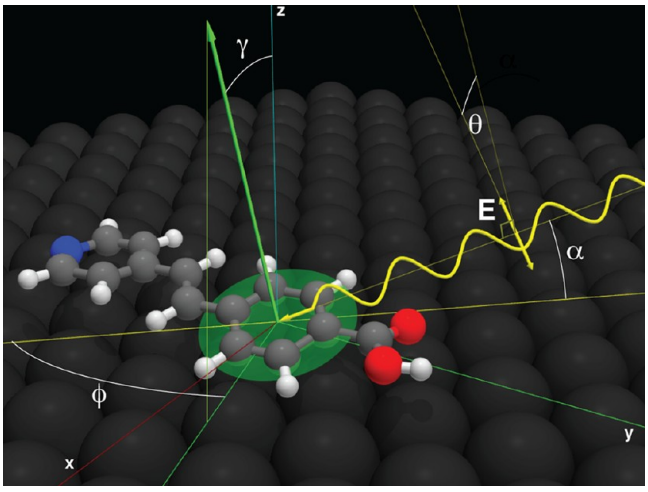

Figure 2. The experimental geometry of the ALOISA beamline. Linearly polarized radiation falls upon the sample with grazing incidence at fixed angle α. The sample can be rotated about the beam axis to change the angle (θ) between the polarization vector and the sample surface. The angles γ and φ respectively represent the polar and azimuthal angles formed by the π^* orbital of a particular ring structure with respect to the substrate coordinate system.

incidence angle α, in partial electron yield mode by means of a channeltron detector with constant retarding voltages of 240 and 370 V when measuring at the C and N edges respectively, between the sample and detector. Simultaneous acquisition of the drain current on the last refocusing mirror (I_0) allowed us to obtain a normalization to the intensity of the incoming beam, as well as an absolute energy calibration by comparing the spectral lines due to carbon and nitrogen contamination of the refocusing mirror with reference absorption

dx.doi.org/10.1021/la303010p | Langmuir 2012, 28, 14291−14300

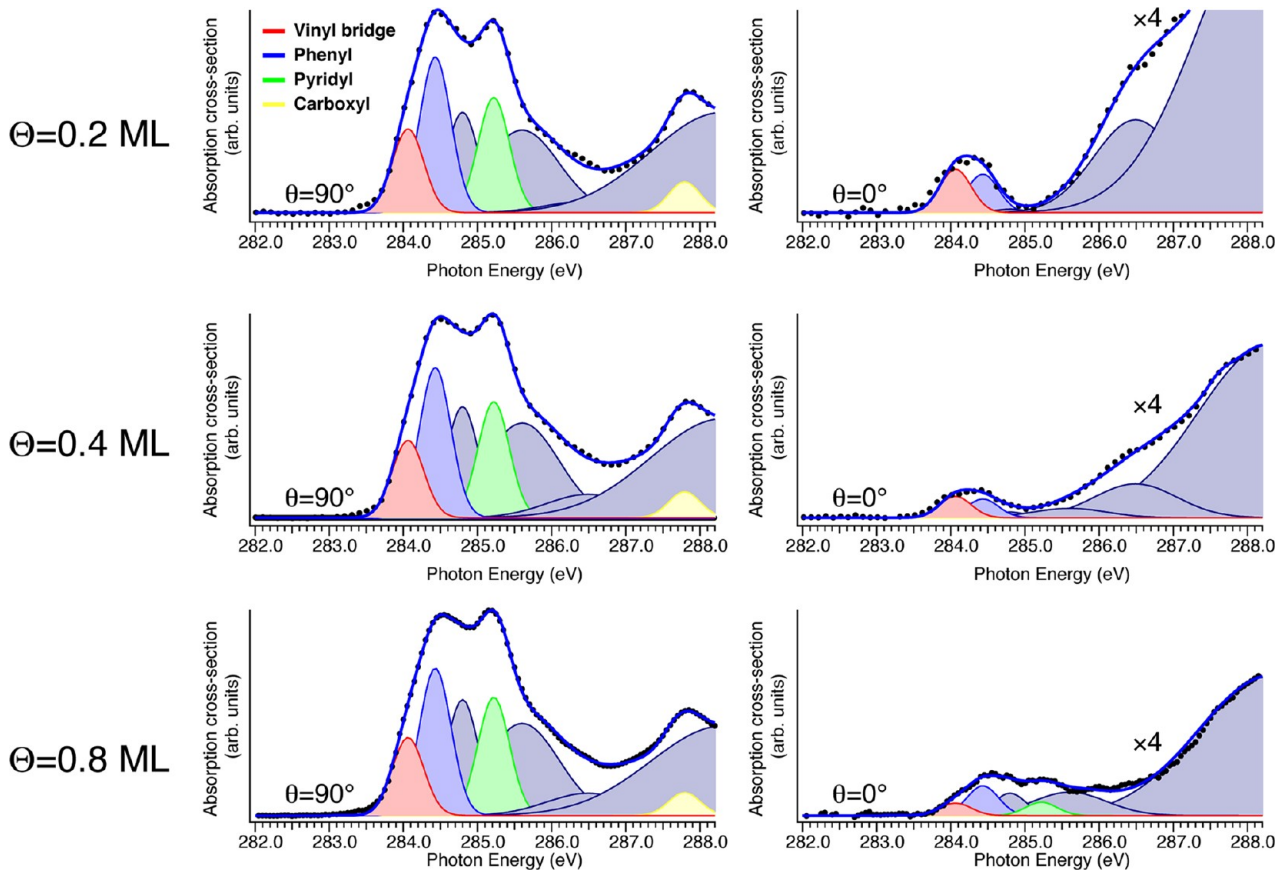

Figure 3. Normalized C K-edge spectra for PVBA twin line structures on Ag(111) as a function of coverage (Θ, in monolayers), using s- (θ = 0°) and p- (θ = 90°) polarizations. The spectra were fitted as a sum of Gaussian lineshapes to identify the specific atoms responsible for each C 1s→π* transition following the calculated spectrum in Figure 4. For clarity, the spectra at θ = 0° have been scaled up by a factor of 4 with respect to the spectra at θ = 90°.

spectra taken with an in-line gas ionization cell.[49] The spectra were further normalized with respect to the C and N K-edge spectra taken from the clean surface prior to each PVBA deposition. Polarization-dependent measurements were performed by rotating the sample about the beam axis, changing the angle (θ) of the polarization vector with respect to the sample surface, while keeping the grazing incidence angle fixed (see Figure 2).

Ab initio calculations were carried out by Kosugi's GSCF3 package.[50] This approach is based on the ab initio improved virtual orbital (IVO) approximation, which explicitly includes the core hole in the Hartree−Fock Hamiltonian.[51] This approximation is effective at the simulation of core excitation spectra of organic molecules.[52−55] IVO calculations are particularly effective for transitions below and near the ionization potential, where the NEXAFS spectra of PVBA show the most distinctive features.

The core excitation spectra of second row elements of the periodic table simulated within the IVO approximation are systematically shifted to higher energy by 2−3 eV and show a "stretch", where higher energy features appear with a greater shift than lower energy features. This has been explored empirically[52,53] and is attributed to overscreening of the core hole in the IVO calculations.[53]

The geometries used for these calculations were provided by ab initio geometry optimization at the HF/6-31G* level, by the SPARTAN 08 program.[56] Calculations of vibrational frequencies were performed to ensure that the geometries were minimum structures (no imaginary frequencies). For the IVO calculations with GSCF3, we used the basis functions of Huzinaga et al.,[57] with a double-ζ basis set expansion scheme on hydrogen (41) and second row elements (carbon, nitrogen, and oxygen) (621 41). A further expansion (411121 3111) is made for each carbon atom which contains a core hole, with an additional *d*-polarization function placed on the core excited carbon (ζ_d = 0.600).

As the calculations are performed on isolated molecules for which the geometry is optimized without restriction, the simulations represent the spectra of gas phase species. Structural changes associated with adsorption on a substrate and the modification of features due to molecule/molecule and molecule/substrate interactions are not accounted for in these calculations. Simulated spectra were obtained from the IVO calculations by broadening each transition as a Gaussian line shape with the program Simile2 package[58] with the following energy dependent full-widths at half-maximum (FWHMs): 0.3 eV FWHM for bound states, 1.0 eV FWHM for states from the ionization energy (IE) to 4 eV above the IE, and 4.0 eV FWHM for states more than 4.0 eV above the IE. These widths are chosen to approximately track the experimental line width observed in the C 1s NEXAFS spectra.

RESULTS AND DISCUSSION

Submonolayer Coverage. Growth of PVBA twin lines (coverage Θ < 0.8 ML) on Ag(111) was investigated by NEXAFS at the C K- and N K-edges (Figures 3 and 5). NEXAFS spectra were recorded with linear polarization angles corresponding to transverse magnetic polarization (TM, p-polarization, θ = 90) and transverse electric (TE, s-polarization, θ=0), with the beam incident along the $\langle 11\bar{2} \rangle$ azimuth of the substrate at a grazing incidence angle α between 5° and 7° (see Figure 2). These experiments were performed at three separate coverages of Θ = 0.2 ML, Θ = 0.4 ML, and Θ = 0.8 ML. The

dx.doi.org/10.1021/la303010p | *Langmuir* 2012, 28, 14291−14300

latter coverage represents the threshold above which the pairing of adjacent lines is lost.

A set of Gaussian lineshapes were used to fit the C K-edge NEXAFS spectra, using an identical number of functions. Photon energy positions and FWHMs were shared between the six spectra, whereas the Gaussian intensities were free to vary. At all coverages, the same set of peaks were used to fit the spectra, as can be seen qualitatively in Figure 3. The uncertainties on the tilt angles extracted from this analysis were added in quadrature with the known tolerances of the beamline (±5°) to determine the overall experimental uncertainty.

To assign the peaks, we compare the experimental data to simulations of the NEXAFS spectrum of PVBA in the gas phase, using the IVO method. A comparison of the resultant calculated spectrum with experiment is presented in Figure 4, where the calculated spectra of the four principal groups of PVBA are plotted separately. The three most intense features in the experimental spectrum can be correlated with the three most intense features of the simulation. We thus identify which portions of the molecule are responsible for a particular resonance peak, and thereby deduce the surface conformation, taking into account the known limitation of this calculation method that stretches the computed energy scale toward higher values. In particular, we may confidently extract the photon energy positions of peaks arising from the vinyl bridge, phenyl and pyridyl rings, and the carboxyl group (see Figure 4).

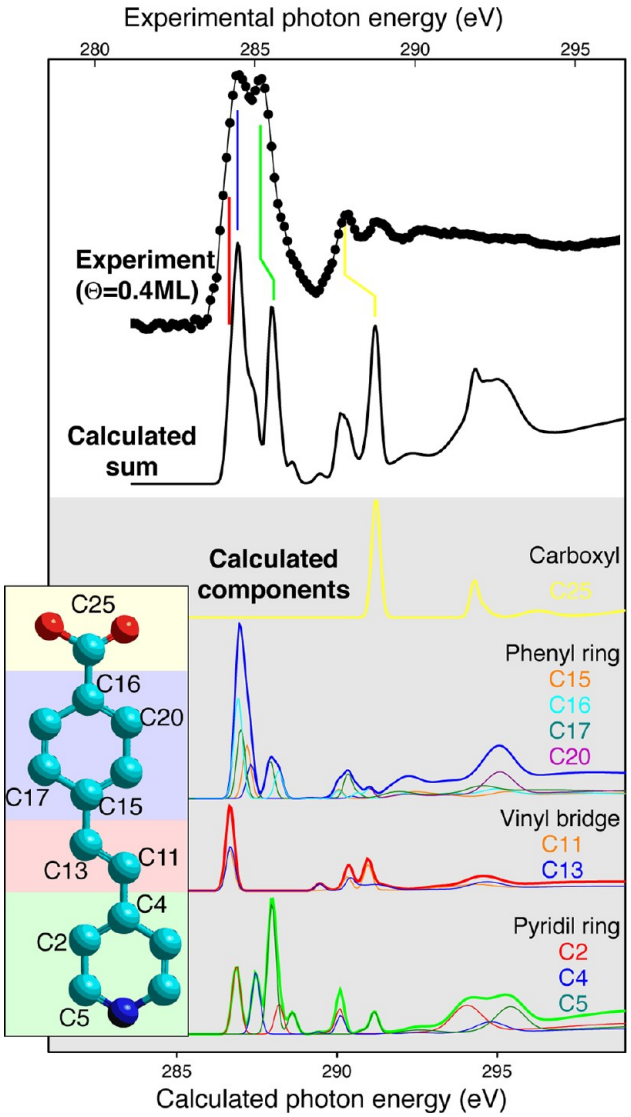

Figure 4. Comparison of experimental and calculated NEXAFS spectra of PVBA (for clarity, the hydrogens have been omitted from the molecular model). The most intense features in the experimental spectrum can be correlated with ones in the calculated spectrum, which elucidates the physical origin for the principal peaks.

From the fits we not only determine the physical origin of the principal peaks, but also the orientation of the adsorbed PVBA (see Figure 2). In the dipole approximation, the integral intensity I for NEXAFS K-edges depends on the direction of the electric field vector with respect to the geometrical orientation of the final state molecular orbital. In aromatic molecules, the π^* orbitals can be treated like vectors normal to the aromatic ring planes, and the intensity I obtained with linear polarized X-ray can be written as[59]

$$I = A \cos^2 \delta \tag{1}$$

where A is the angle-integrated cross section, and δ is the angle between the π^* resonance vector and the polarization vector of the incoming X-ray. According to our experimental geometry and using the angular notation of Figure 2, this equation can be written as

$$I = A(\sin\gamma \cos\phi \sin\alpha \sin\theta + \sin\gamma \sin\phi \cos\theta + \cos\gamma \cos\alpha \sin\theta)^2 \tag{2}$$

where A is the same constant as in eq 1, α is the angle of incidence with respect to the substrate of the incoming X-ray, θ relates to the angle between the photon polarization vector and the sample normal, and γ and ϕ represent the polar and azimuthal angles, respectively, formed by the π^* orbital in question. The c_3 symmetry of the substrate permits us to set $\sin\phi = \cos\phi = 0$, and $\sin^2\phi = \cos^2\phi = 1/2$, in the expansion of eq 2.[59] Thus, we may calculate the tilt angle (γ) of the molecule with respect to the surface using the following relation:[59−61]

$$I = A\left(\sin^2\theta\left(\cos^2\alpha \cos^2\gamma + \frac{1}{2}\sin^2\alpha \sin^2\gamma\right) + \frac{1}{2}\cos^2\theta \sin^2\gamma\right) \tag{3}$$

or, normalizing to the intensity at $\theta = 0°$, as the sample is rotated about the incoming photon beam direction by θ to change the angle between the photon polarization vector and the sample surface:

$$\frac{I(\theta)}{I(0°)} = 1 + \sin^2\theta \cos^2\alpha\left(\frac{2}{\tan^2\gamma} - 1\right) \tag{4}$$

The calculated tilt angles are summarized in Table 1. We observe that at the lowest coverages, the pyridyl ring is adsorbed flat on the surface. The vinyl and phenyl groups are slightly twisted from the gas phase configuration, with a tilt angle of approximately 17° at all three coverages (although there is a significant uncertainty margin on these values). The carboxyl group remains parallel to the surface at all coverages. As the PVBA coverage is increased toward 0.8 ML, the pyridyl gains a tilt of 13 ± 6° at the threshold coverage. This suggests that the entire molecule, save for the carboxyl end that remains flat, is tilted at an angle of 15 ± 3° (weighted average) with

dx.doi.org/10.1021/la303010p | Langmuir 2012, 28, 14291−14300

Table 1. Summary of Calculated Tilt Angles (γ) from the Fits to Experimental Spectra of Figures 3 and 5 (Same Peak Colors Are Used) and Use of Eq 4

peak	energy (eV)	origin	tilt angle (γ) Θ = 0.2 ML	Θ = 0.4 ML	Θ = 0.8 ML
C K (red)	284.1	vinyl bridge	18 ± 10°	20 ± 10°	16 ± 7°
C K (blue)	284.4	phenyl ring	19 ± 10°	14 ± 7°	18 ± 5°
C K (green)	285.2	pyridyl ring	0 ± 5°	0 ± 5°	13 ± 6°
C K (yellow)	287.8	COOH tail	0 ± 5°	0 ± 5°	0 ± 5°
N K (blue)	398.6	pyridyl ring	0 ± 5°	0 ± 5°	13 ± 5°

respect to the surface, indicating a relaxation to a more planar geometry.

The NEXAFS experiment was also performed at the N K-edge in s- and p-polarization orientations, and the results are presented in Figure 5. The N K-edge is particularly helpful in this analysis, because the N 1s→π^* resonance peak located at 398.6 eV can be considered to be localized exclusively on the pyridil ring, and thus unambiguously assigns an orientation for this end of the molecule. The low photon energy π^* resonance (blue) is observed at all coverages in p-polarization ($\theta = 0$) in Figure 5. The intensity of the resonance vanishes for s-polarization ($\theta = 90$) when the coverage is below Θ = 0.8 ML, and at or above this coverage the tilt of the pyridyl ring is calculated to be 13 ± 5°, using the shaded region indicated in Figure 5. This value is in agreement with the data obtained from the C1s→π^* resonance, and gives us confidence in our assignment of peaks above. The tilt is notably less than for pure pyridine on this substrate, which adsorbs with the nitrogen atom pointing toward the surface.[62] The overall conclusion from the N K-edge is the same: the pyridyl ring is flat for coverages up to the threshold coverage, at which point it takes on a slight tilt with respect to the surface normal. We note that the photon energy positions and FWHM of the π^* resonances are identical throughout this coverage range, indicating that there is no change in the interaction between the nitrogen atom and the underlying silver lattice as the coverage is increased.[59]

Following the proposed STM model for the twinned lines, we may interpret the consequences of the measured molecular twisting. Each PVBA molecule in the twinned chain is engaged in two chaining head-to-tail hydrogen bonds with its neighbors and weak lateral attractions between carbonyl and pyridyl moieties. Within the chain unit cell we use the labeling in Figure 6, these are H1···N1 and H2···O1. With the molecules placed as determined by STM results[35] and producing the above-determined tilt angles through a combination of dihedral rotations, for the low coverages the bond lengths are 2.6 Å and 2.0 Å for O1···N1 and H2···O1, respectively. As the coverage is increased and the pyridyl end rotates out of plane, the H2···O1 distance is increased to 2.5 ± 0.2 Å. The increased bond length can be associated with a weakening of the carbonyl−pyridyl bond,[63,64] which in turn reduces the stability of the twin chains. The cause of the weakening is likely to be due to the proximity of other PVBA molecules in the voids between each twin line pair, which must be accommodated at these higher coverages. Thus, we conclude that the overall torsion of the molecule at low coverage is necessary for placing H2 and O1 at a distance appropriate for the formation of the hydrogen bond that twins the chains, and thus a key stabilizing element of this surface structure. At coverages with Θ > 0.8 ML, the increased tilt of the pyridyl tail moves H2 to a further distance from O1, and hence the lateral attraction is weakened, which is corroborated by the changed appearance observed in high coverage STM measurements. Despite the planarity of the phenyl, vinyl, and pyridyl groups at moderate coverages, there remains a significant twist in the carboxyl end, which remains parallel to the surface. This may be indicative of the remaining head−tail linear bonding, representing the prevailing interaction in the twin chains, still observed above the threshold coverage.

Multilayer Coverage. To investigate the saturation behavior of PVBA on Ag(111), we prepared a surface with a much higher coverage, on the order of 5.0 ML (estimated lower limit from the XPS signal, see Supporting Information).

NEXAFS scans were performed at C−K and N−K edges to determine whether any preferred molecular orientation exists at these higher coverages, even though the surface ordering is weak. The spectra and peak deconvolutions are presented in Figure 7.

The decomposition of the C K-edge NEXAFS shown in Figure 7 (a and b) is summarized in Table 2. The same set of peaks used for the submonolayer surfaces is used, with no appreciable change in energy position. The molecule appears to be completely tilted with respect to the substrate normal by an average angle of 24 ± 3°. We may conclude that despite the loss of in-plane order at these higher coverages, PVBA returns to a planar conformation, albeit tilted with respect to the supporting surface.

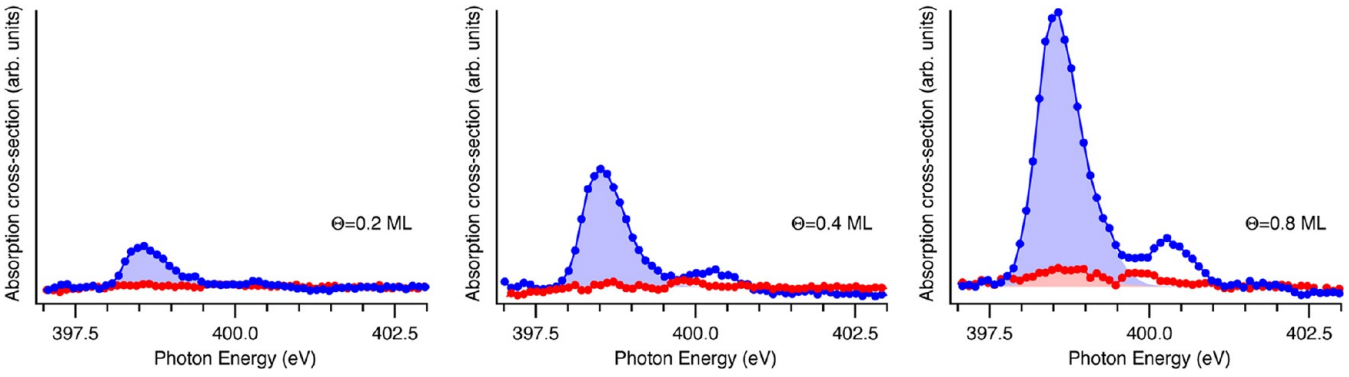

Figure 5. The π^* region for NEXAFS at the N K-edge in both s- (red) and p- (blue) polarizations, at three coverages. The shaded region is used to calculate the tilt angle.

dx.doi.org/10.1021/la303010p | Langmuir 2012, 28, 14291−14300

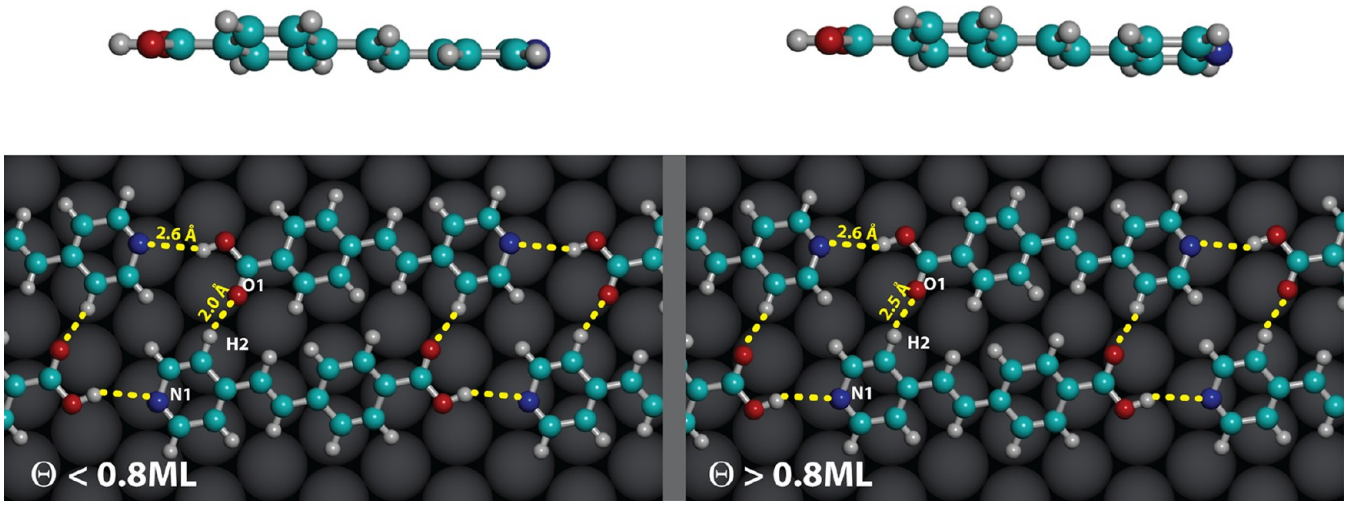

Figure 6. Molecular model for the twinned line system, at low and high coverages. The stabilizing hydrogen interactions of the twinned chains are marked by the yellow dashed lines and annotated with the determined hydrogen bond lengths. The top insets show side profiles of the molecule to highlight the twisted adsorption geometry.

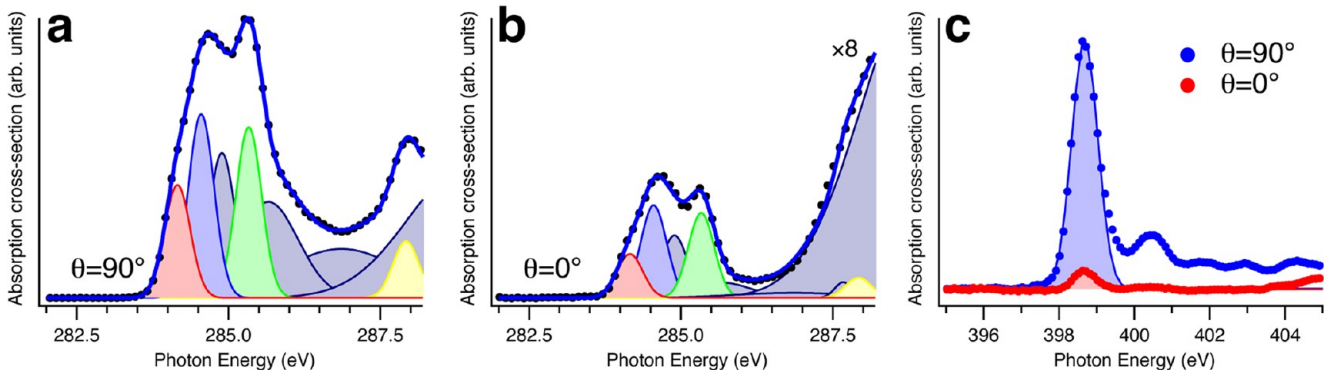

Figure 7. NEXAFS from the multilayer surface, measured at (a) the C 1s edge with $\theta = 90°$ (p-polarization), (b) the C 1s edge with $\theta = 0°$ (s-polarization) (for clarity data have been scaled up by a factor of 8), and (c) N 1s, in both polarizations.

Table 2. Summary of Deconvolution for N1s and C1s NEXAFS Spectra from the Multilayer Surface

peak	energy (eV)	origin	tilt angle (γ)
C K (red)	284.2	vinyl bridge	24 ± 5°
C K (blue)	284.5	phenyl ring	27 ± 5°
C K (green)	285.3	pyridyl ring	26 ± 5°
C K (yellow)	287.9	COOH tail	23 ± 7°
N K (blue)	398.7	pyridyl	19 ± 5°

Annealing the PVBA/Ag submonolayer surfaces at 375 K produces a subtle but important change in the C 1s core level XPS spectra shown in Figure 8, where a comparison can be made for identical nominal coverages of PVBA from a deposition done at (a) room temperature and (b) after annealing to 100 °C for 5 min. The only significant change is the shift of the highest energy peak (blue) from 288.7 eV to 287.5 eV after annealing. This peak is associated with the carbon in the carboxylic acid group, and its shift to lower binding energy is associated with deprotonation, consistent with prior observations in similar building blocks.[65,66] Deprotonation of PVBA has been reported on the more reactive low-index faces of copper,[39,44,67−69] where PVBA packs into a variety of structures driven largely by molecule-surface interactions or metal coordination. Deprotonation of PVBA was additionally reported on Ag(110) following thermal annealing, but in this case the molecules bind to the step edges.[38] In this case, the removal of the acid group's hydrogen necessitates the loss of the H-bond responsible for maintaining the head−tail structure of the chains.[70]

NEXAFS scans at the C K-edge reveal subtle changes in geometry for the deprotonated molecules, as shown in Figure 9. In Figure 9a we find a comparison of the NEXAFS from intact and deprotonated PVBA/Ag systems, at identical coverages. The same set of peaks used for the submonolayer surfaces is used, except that every peak centroid is shifted to higher excitation energy by 100 meV. Simple aromatic hydrocarbons also exhibit similar shifts in their absorption spectra when transitioning from gas-phase to clusters in the solid state,[71,72] although it is not known what role the surface plays in our case. Close inspection of the deconvoluted peaks shows that the entire molecule is twisted by an angle of 16 ± 3° from the surface normal, except for the COO^- tail, which twists to 25 ± 5° from the surface normal. Therefore, the only change from the 0.8 ML coverage of intact PVBA is that the carboxyl has lost its coplanar orientation with the surface, as might be expected since the H1···N1 bond can no longer exist.

Surprisingly, we detect no loss of order in the structure: RHEED images (see Supporting Information) before and after annealing show no appreciable symmetry change post

dx.doi.org/10.1021/la303010p | Langmuir 2012, 28, 14291−14300

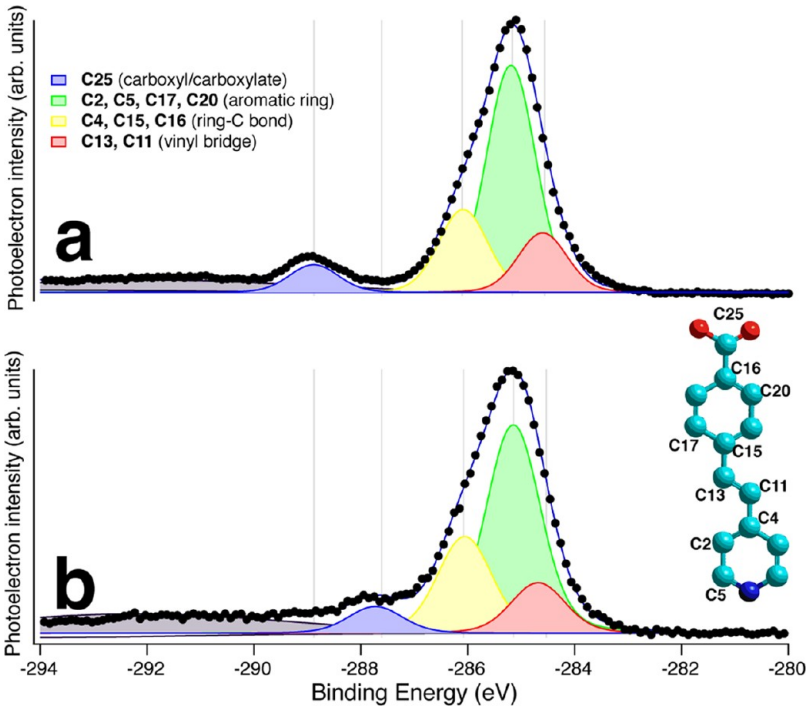

Figure 8. (a) Carbon 1s core level measured from a surface with 0.8 ML of PVBA. (b) Carbon 1s core level measured from a similar surface after annealing to 100 °C.

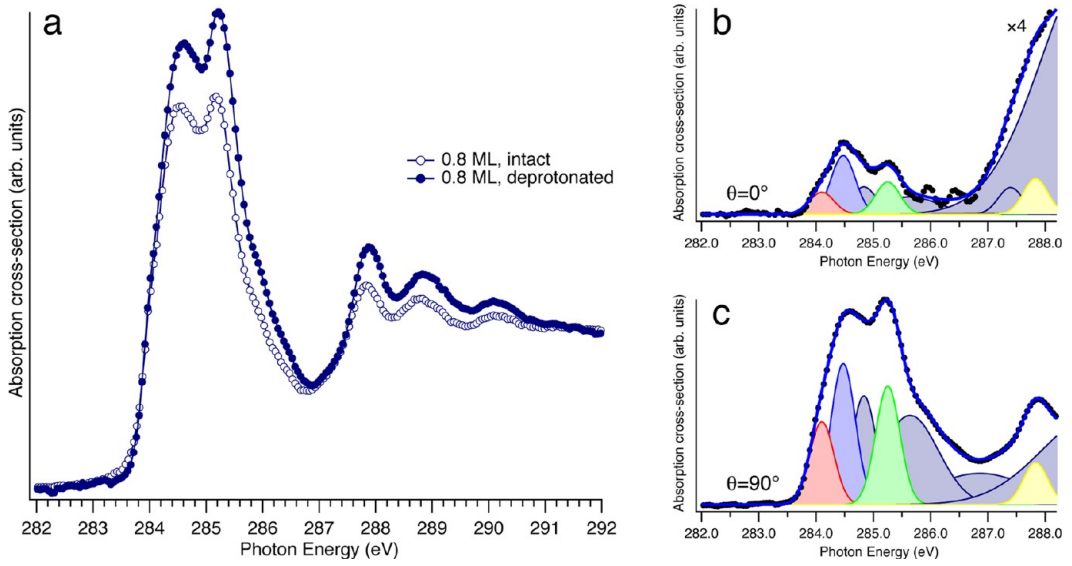

Figure 9. (a) NEXAFS at the C1s edge in p-polarization for unannealed (intact) and annealed (deprotonated) PVBA surfaces. Deconvolution of the annealed surface spectra is shown for (b) $\theta = 90°$ and (c) $\theta = 0°$.

deprotonation. This suggests that while hydrogen bonding may be responsible for the initial positioning of PVBA into twinned lines, their stability may be additionally enhanced by interaction with the substrate. Moreover, it may be the case that following deprotonation, the twisting observed in the carboxylate moiety represents a rebonding to surface atoms, anchoring the molecules in place: this could explain the apparent lack of reordering after the hydrogen bonding is disrupted.

■ CONCLUSIONS AND PERSPECTIVES

We performed NEXAFS measurements on self-assembled one-dimensional chains of PVBA molecules on the (111) surface of silver. The results confirmed and extended previous STM results from the same system. For submonolayer coverages below the threshold of 0.8 ML, angle-dependent NEXAFS measurements at the C K-edge indicate that PVBA adsorbs in a twisted geometry on Ag(111), with the pyridyl and carboxyl moieties parallel to the surface, and with the phenyl group and vinyl bridge twisted out of plane by approximately 17°. The consequence of this twist is to permit the interchain bonding that stabilizes the twin chains in the low coverage phase. Above the threshold coverage, the entire molecule is tilted by 15 ± 3° with respect to the surface normal, save for the carboxyl moiety, which remains parallel to the substrate. At multilayer coverage the geometry is altered, with the entire molecule tilted by 24 ±

dx.doi.org/10.1021/la303010p | *Langmuir* 2012, 28, 14291−14300

3° to the surface normal. These observations provide an independent spectroscopic verification of the conclusions drawn from STM measurements,[34−37,41] and provides a new insight into the stabilizing forces for this overlayer system. A brief annealing at 100 °C causes the carboxyl group to deprotonate. However, the geometry of the molecule is essentially unchanged: the carboxyl group, no longer H-bonded to adjacent PVBA molecule, twists out of the surface plane presumably to form an anchor with the substrate, locking the line geometry in place even though the original organizing force has been suppressed.

■ ASSOCIATED CONTENT

Ⓢ Supporting Information

XPS measurements and RHEED patterns. This material is available free of charge via the Internet at http://pubs.acs.org.

■ AUTHOR INFORMATION

Corresponding Author

*E-mail: rosei@emt.inrs.ca.

Author Contributions

◆These authors contributed equally to this work.

Notes

The authors declare no competing financial interest.

■ ACKNOWLEDGMENTS

This work was partly supported by NSERC of Canada (Discovery Grants). F.R. acknowledges the Canada Research Chairs program for partial salary support. The authors are grateful to Katharina Diller as well as Drs. Dmitrii Perepichka and Rico Gutzler for helpful discussions during the preparation of the manuscript.

■ REFERENCES

(1) Cicoira, F.; Santato, C.; Rosei, F. Two-dimensional nanotemplates as surface cues for the controlled assembly of organic molecules. In *STM and AFM Studies On (Bio)Molecular Systems: Unravelling the Nanoworld*; Samori, P., Ed.; Springer-Verlag: New York, 2008; Vol. *285*, pp 203−267.

(2) De Feyter, S.; De Schryver, F. C. Two-dimensional supramolecular self-assembly probed by scanning tunneling microscopy. *Chem. Soc. Rev.* **2003**, *32* (3), 139−150.

(3) Ivasenko, O.; MacLeod, J. M.; Chernichenko, K. Y.; Balenkova, E. S.; Shpanchenko, R. V.; Nenajdenko, V. G.; Rosei, F.; Perepichka, D. F. Supramolecular assembly of heterocirculenes in 2D and 3D. *Chem. Commun.* **2009**, *10*, 1192−1194.

(4) Kuhnle, A.; Molina, L. M.; Linderoth, T. R.; Hammer, B.; Besenbacher, F. Growth of unidirectional molecular rows of cysteine on Au(110)-(1 × 2) driven by adsorbate-induced surface rearrangements. *Phys. Rev. Lett.* **2004**, *93*, 8.

(5) MacLeod, J. M.; Ivasenko, O.; Fu, C.; Taerum, T.; Rosei, F.; Perepichka, D. F. Supramolecular Ordering in Oligothiophene-Fullerene Monolayers. *J. Am. Chem. Soc.* **2009**, *131* (46), 16844−16850.

(6) Palma, C.-A.; Samori, P. Blueprinting macromolecular electronics. *Nat. Chem.* **2011**, *3* (6), 431−436.

(7) Rosei, F.; Schunack, M.; Naitoh, Y.; Jiang, P.; Gourdon, A.; Laegsgaard, E.; Stensgaard, I.; Joachim, C.; Besenbacher, F. Properties of large organic molecules on metal surfaces. *Prog. Surf. Sci.* **2003**, *71* (5−8), 95−146.

(8) Smith, R. K.; Lewis, P. A.; Weiss, P. S. Patterning self-assembled monolayers. *Prog. Surf. Sci.* **2004**, *75* (1−2), 1−68.

(9) Xu, S.; Dong, M.; Rauls, E.; Otero, R.; Linderoth, T. R.; Besenbacher, F. Coadsorption of guanine and cytosine on graphite: Ordered structure based on GC pairing. *Nano Lett.* **2006**, *6* (7), 1434−1438.

(10) Xu, W.; Dong, M.; Gersen, H.; Rauls, E.; Vazquez-Campos, S.; Crego-Calama, M.; Reinhoudt, D. N.; Stensgaard, I.; Laegsgaard, E.; Linderoth, T. R.; Besenbacher, F. Cyanuric acid and metamine on Au(111): Structure and energetics of hydrogen-bonded networks. *Small* **2007**, *3* (5), 854−858.

(11) Amabilino, D. B.; De Feyter, S.; Lazzaroni, R.; Gomar-Nadal, E.; Veciana, J.; Rovira, C.; Abdel-Mottaleb, M. M.; Mamdouh, W.; Iavicoli, P.; Psychogyiopoulou, K.; Linares, M.; Minoia, A.; Xu, H.; Puigmarti-Luis, J. Monolayer self-assembly at liquid−solid interfaces: Chirality and electronic properties of molecules at surfaces. *J. Phys.: Condens. Matter* **2008**, *20* (18), 184003.

(12) Barth, J. V.; Weckesser, J.; Lin, N.; Dmitriev, A.; Kern, K. Supramolecular architectures and nanostructures at metal surfaces. *Appl. Phys. A: Mater. Sci. Process.* **2003**, *76* (5), 645−652.

(13) Barth, J. V. Molecular architectonic on metal surfaces. *Annu. Rev. Phys. Chem.* **2007**, *58*, 375−407.

(14) Giancarlo, L. C.; Flynn, G. W. Raising flags: Applications of chemical marker groups to study self-assembly, chirality, and orientation of interfacial films by scanning tunneling microscopy. *Acc. Chem. Res.* **2000**, *33* (7), 491−501.

(15) Ernst, K.-H. Supramolecular Surface Chirality. In *Supramolecular Chirality*; Springer: Berlin, 2006; Vol. *265*, pp 209−252.

(16) Nath, K. G.; Ivasenko, O.; MacLeod, J. M.; Miwa, J. A.; Wuest, J. D.; Nanci, A.; Perepichka, D. F.; Rosei, F. Crystal engineering in two dimensions: an approach to molecular nanopatterning. *J. Phys. Chem. C* **2007**, *111*, 16996−17007.

(17) Cicoira, F.; Santato, C. Organic light emitting field effect transistors: Advances and perspectives. *Adv. Funct. Mater.* **2007**, *17* (17), 3421−3434.

(18) Contini, G.; Gori, P.; Ronci, F.; Zema, N.; Colonna, S.; Aschi, M.; Palma, A.; Turchini, S.; Catone, D.; Cricenti, A.; Prosperi, T. Chirality Transfer from a Single Chiral Molecule to 2D Superstructures in Alaninol on the Cu(100) Surface. *Langmuir* **2011**, *27* (12), 7410−7418.

(19) Koller, G.; Berkebile, S.; Ivanco, J.; Netzer, F. P.; Ramsey, M. G. Device relevant organic films and interfaces: A surface science approach. *Surf. Sci.* **2007**, *601* (24), 5683−5689.

(20) Dadvand, A.; Cicoira, F.; Chernichenko, K. Y.; Balenkova, E. S.; Osuna, R. M.; Rosei, F.; Nenajdenko, V. G.; Perepichka, D. F. Heterocirculenes as a new class of organic semiconductors. *Chem. Commun.* **2008**, *42*, 5354−5356.

(21) Brusso, J. L.; Hirst, O. D.; Dadvand, A.; Ganesan, S.; Cicoira, F.; Robertson, C. M.; Oakley, R. T.; Rosei, F.; Perepichkat, D. F. Two-dimensional structural motif in thienoacene semiconductors: Synthesis, structure, and properties of tetrathienoanthracene isomers. *Chem. Mater.* **2008**, *20* (7), 2484−2494.

(22) Dadvand, A.; Moiseev, A. G.; Sawabe, K.; Sun, W.-H.; Djukic, B.; Chung, I.; Takenobu, T.; Rosei, F.; Perepichka, D. F. Maximizing field-effect mobility and solid-state luminescence in organic semiconductors. *Angew. Chem., Int. Ed.* **2012**, *51* (16), 3837−3841.

(23) Jeeva, S.; Lukoyanova, O.; Karas, A.; Dadvand, A.; Rosei, F.; Perepichka, D. F. Highly emissive and electrochemically stable thienylene vinylene oligomers and copolymers: An unusual effect of alkylsulfanyl substituents. *Adv. Funct. Mater.* **2010**, *20* (10), 1661−1669.

(24) Sun, T. L.; Han, D.; Rhemann, K.; Chi, L. F.; Fuchs, H. Stereospecific interaction between immune cells and chiral surfaces. *J. Am. Chem. Soc.* **2007**, *129* (6), 1496−1497.

(25) Solladie, G.; Zimmermann, R. G. Liquid-crystals - A tool for studies on chirality. *Angew. Chem., Int. Ed. Engl.* **1984**, *23* (5), 348−362.

(26) Li, G.; Shinar, J. Combinatorial fabrication and studies of bright white organic light-emitting devices based on emission from rubrene-doped 4,4′-bis(2,2′-diphenylvinyl)-1,1′-biphenyl. *Appl. Phys. Lett.* **2003**, *83* (26), 5359−5361.

(27) Takahashi, T.; Takenobu, T.; Takeya, J.; Iwasa, Y. Ambipolar organic field-effect transistors based on rubrene single crystals. *Appl. Phys. Lett.* **2006**, *88*, 3.
(28) Podzorov, V.; Menard, E.; Borissov, A.; Kiryukhin, V.; Rogers, J. A.; Gershenson, M. E. Intrinsic charge transport on the surface of organic semiconductors. *Phys. Rev. Lett.* **2004**, *93*, 8.
(29) Kafer, D.; Ruppel, L.; Witte, G.; Woll, C. Role of molecular conformations in rubrene thin film growth. *Phys. Rev. Lett.* **2005**, *95*, 16.
(30) Cai, C. Z.; Bosch, M. M.; Muller, B.; Tao, Y.; Kundig, A.; Bosshard, C.; Gan, Z. H.; Biaggio, I.; Liakatas, I.; Jager, M.; Schwer, H.; Gunter, P. Oblique incidence organic molecular beam deposition and nonlinear optical properties of organic thin films with a stable in-plane directional order. *Adv. Mater.* **1999**, *11* (9), 745−749.
(31) Cai, C. Z.; Muller, B.; Weckesser, J.; Barth, J. V.; Tao, Y.; Bosch, M. M.; Kundig, A.; Bosshard, C.; Biaggio, I.; Gunter, P. Model for in-plane directional ordering of organic thin films by oblique incidence organic molecular beam deposition. *Adv. Mater.* **1999**, *11* (9), 750−754.
(32) Tapponnier, A.; Delvigne, E.; Biaggio, I.; Gunter, P. Nonlinear optical and structural properties of noncentrosymmetric organic thin films obtained by oblique incidence molecular beam deposition. *J. Opt. Soc. Am. B: Opt. Phys.* **2004**, *21* (3), 685−690.
(33) Kim, B. I. Chiral recognition of PVBA on Pd(111) and Ag(111) surfaces. *Langmuir* **2006**, *22* (22), 9272−9280.
(34) Weckesser, J.; De Vita, A.; Barth, J. V.; Cai, C.; Kern, K. Mesoscopic correlation of supramolecular chirality in one-dimensional hydrogen-bonded assemblies. *Phys. Rev. Lett.* **2001**, *87* (9), 096101.
(35) Barth, J. V.; Weckesser, J.; Cai, C. Z.; Gunter, P.; Burgi, L.; Jeandupeux, O.; Kern, K. Building supramolecular nanostructures at surfaces by hydrogen bonding. *Angew. Chem., Int. Ed.* **2000**, *39* (7), 1230−1234.
(36) Weckesser, J.; Barth, J. V.; Cai, C. Z.; Müller, B.; Kern, K. Binding and ordering of large organic molecules on an anisotropic metal surface: PVBA on Pd(110). *Surf. Sci.* **1999**, *431* (1−3), 168−173.
(37) Weckesser, J.; Barth, J. V.; Kern, K. Direct observation of surface diffusion of large organic molecules at metal surfaces: PVBA on Pd(110). *J. Chem. Phys.* **1999**, *110* (11), 5351−5354.
(38) Pascual, J. I.; Barth, J. V.; Ceballos, G.; Trimarchi, G.; De Vita, A.; Kern, K.; Rust, H. P. Mesoscopic chiral reshaping of the Ag(110) surface induced by the organic molecule PVBA. *J. Chem. Phys.* **2004**, *120* (24), 11367−11370.
(39) Vidal, F.; Delvigne, E.; Stepanow, S.; Lin, N.; Barth, J. V.; Kern, K. Chiral Phase Transition in Two-Dimensional Supramolecular Assemblies of Prochiral Molecules. *J. Am. Chem. Soc.* **2005**, *127*, 10101−10106.
(40) Barth, J. V.; Weckesser, J.; Trimarchi, G.; Vladimirova, M.; De Vita, A.; Cai, C. Z.; Brune, H.; Gunter, P.; Kern, K. Stereochemical effects in supramolecular self-assembly at surfaces: 1-D versus 2-D enantiomorphic ordering for PVBA and PEBA on Ag(111). *J. Am. Chem. Soc.* **2002**, *124* (27), 7991−8000.
(41) Weckesser, J. *Atomic Scale Observations of Large Organic Molecules at Metal Surfaces: Bonding, Ordering and Supramolecular Self-Assembly*; Ecole Polytechnique Fédérale de Lausanne: Lausanne, Switzerland, 2000.
(42) Pivetta, M.; Blum, M. C.; Patthey, F.; Schneider, W. D. Three-dimensional chirality transfer in rubrene multilayer islands on Au(111). *J. Phys. Chem. B* **2009**, *113*, 4578−4581.
(43) Vidal, F.; Delvigne, E.; Stepanow, S.; Lin, N.; Barth, J. V.; Kern, K. Chiral phase transition in two-dimensional supramolecular assemblies of prochiral molecules. *J. Am. Chem. Soc.* **2007**, *127* (28), 10101−10106.
(44) Lin, N.; Stepanow, S.; Vidal, F.; Barth, J. V.; Kern, K. Manipulating 2D metal-organic networks via ligand control. *Chem. Commun.* **2005**, *13*, 1681−1683.
(45) Kim, B. I.; Cai, C. Z.; Deng, X. B.; Perry, S. S. Adsorption-induced chirality influences surface orientation in organic self-assembled structures: An STM study of PVBA on Pd(111). *Surf. Sci.* **2003**, *538* (1−2), 45−52.
(46) Klappenberger, F.; Canas-Ventura, M. E.; Clair, S.; Pons, S.; Schlickum, U.; Qu, Z. R.; Brune, H.; Kern, K.; Strunskus, T.; Woll, C.; Comisso, A.; De Vita, A.; Ruben, M.; Barth, J. V. Conformational adaptation in supramolecular assembly on surfaces. *ChemPhysChem* **2007**, *8*, 1782−1786.
(47) Klappenberger, F.; Canas-Ventura, M. E.; Clair, S.; Pons, S.; Schlickum, U.; Qu, Z. R.; Strunskus, T.; Comisso, A.; Woll, C.; Brune, H.; Kern, K.; De Vita, A.; Ruben, M.; Barth, J. V. Does the surface matter? Hydrogen-bonded chain formation of an oxalic amide derivative in a two- and three-dimensional environment. *ChemPhysChem* **2008**, *9* (17), 2522−2530.
(48) Schlickum, U.; Decker, R.; Klappenberger, F.; Zoppellaro, G.; Klyatskaya, S.; Auwärter, W.; Neppl, S.; Kern, K.; Brune, H.; Ruben, M.; Barth, J. V. Chiral Kagomé Lattice from Simple Ditopic Molecular Bricks. *J. Am. Chem. Soc.* **2008**, 130.
(49) Floreano, L.; Naletto, G.; Cvetko, D.; Gotter, R.; Malvezzi, M.; Marassi, L.; Morgante, A.; Santaniello, A.; Verdini, A.; Tommasini, F.; Tondello, G. Performance of the grating-crystal monochromator of the ALOISA beamline at the Elettra Synchrotron. *Rev. Sci. Instrum.* **1999**, *70* (10), 3855−3864.
(50) Kosugi, N.; Kuroda, H. Efficient methods for solving the open-shell SCF problem and for obtaining an initial guess - The one-Hamiltonian and the partial SCF methods. *Chem. Phys. Lett.* **1980**, *74* (3), 490−493.
(51) Hunt, W. J.; Goddard, W. A. Excited States of H_2O using improved virtual orbitals. *Chem. Phys. Lett.* **1969**, *3* (6), 414−418.
(52) Urquhart, S. G.; Ade, H. Trends in the carbonyl core (C 1S, O 1S) → $\pi^*_{c=o}$ transition in the near-edge X-ray absorption fine structure spectra of organic molecules. *J. Phys. Chem. B* **2002**, *106* (34), 8531−8538.
(53) Cooney, R. R.; Urquhart, S. G. Chemical trends in the near-edge X-ray absorption fine structure of monosubstituted and para-bisubstituted benzenes. *J. Phys. Chem. B* **2004**, *108* (47), 18185−18191.
(54) Otero, E.; Urquhart, S. G. Nitrogen 1s near-edge X-ray absorption fine structure spectroscopy of amino acids: Resolving zwitterionic effects. *J. Phys. Chem. A* **2006**, *110* (44), 12121−12128.
(55) Ueda, K.; Okunishi, M.; Chiba, H.; Shimizu, Y.; Ohmori, K.; Sato, Y.; Shigemasa, E.; Kosugi, N. Rydberg-valence mixing in the C-1s excited-states of CH_4 probed by electron-spectroscopy. *Chem. Phys. Lett.* **1995**, *236* (3), 311−317.
(56) *Spartan '94*; Wavefunction Inc.: Irvine, CA, 1994.
(57) Huzinaga, S.; Andzelm, J.; Klobokowski, M.; Radzio-Andzelm, E.; Sasaki, Y.; Tatewaki, H. *Gaussian Basis Sets for Molecular Calculations*; Elsevier: Amsterdam, 1984.
(58) Huo, B. H.; Hitchcock, A. P. *Simile2*, McMaster University: Hamilton, ON, 1996.
(59) Stöhr, J. *NEXAFS Spectroscopy*; Springer-Verlag: Berlin/Heidelberg/New York, 1996.
(60) Mainka, C.; Bagus, P. S.; Schertel, A.; Strunskus, T.; Grunze, M.; Woll, C. Linear dichroism in X-ray-absorption spectroscopy of strongly chemisorbed planar molecules - Role of adsorption induced rehybridizations. *Surf. Sci.* **1995**, *341* (3), L1055−L1060.
(61) Reichert, J.; Schiffrin, A.; Auwärter, W.; Weber-Bargioni, A.; Marschall, M.; Dell'Angela, M.; Cvetko, D.; Bavdek, G.; Cossaro, A.; Morgante, A.; Barth, J. V. L-Tyrosine on Ag(111): Universality of the amino acid 2D zwitterionic bonding scheme? *ACS Nano* **2010**, *4* (2), 1218−1226.
(62) Bader, M.; Haase, J.; Frank, K. H.; Ocal, C.; Puschmann, A. Near-edge X-ray absorption fine-structure studies of ring molecules adsorbed on single crystal surfaces. *J. Phys. Colloq.* **1986**, *47* (C8), C8−491-C8−496.
(63) Fourmigué, M.; Batail, P. Activation of hydrogen- and halogen-bonding interactions in tetrathiafulvalene-based crystalline molecular conductors. *Chem. Rev.* **2004**, *104*, 39.
(64) Desiraju, G. R. The C−H···O hydrogen bond: Structural implications and supramolecular design. *Acc. Chem. Res.* **1996**, *29*, 441.

(65) Stepanow, S.; Strunskus, T.; Lingenfelder, M.; Dmitriev, A.; Spillmann, H.; Lin, N.; Barth, J. V.; Wöll, C.; Kern, K. Deprotonation-driven phase transformations in terephthalic acid self-assembly on Cu(100). *J. Phys. Chem. B* **2004**, *108* (50), 19392−19397.
(66) Canas-Ventura, M. E.; Klappenberger, F.; Clair, S.; Pons, S.; Kern, K.; Brune, H.; Strunskus, T.; Woll, C.; Fasel, R.; Barth, J. V. Coexistence of one- and two-dimensional supramolecular assemblies of terephthalic acid on Pd(111) due to self-limiting deprotonation. *J. Chem. Phys.* **2006**, *125* (18), 184710.
(67) Ohmann, R.; Vitali, L.; Kern, K. Actuated transitory metal−ligand bond as tunable electromechanical switch. *Nano Lett.* **2010**, *10* (8), 2995−3000.
(68) Vitali, L.; Levita, G.; Ohman, R.; Comisso, A.; De Vita, A.; Kern, K. Portrait of the potential barrier at metal−organic nanocontacts. *Nat. Mater.* **2010**, *9*, 320−323.
(69) Ohman, R.; Levita, G.; Vitali, L.; De Vita, A.; Kern, K. Influence of subsurface layers on the adsorption of large organic molecules on close-packed metal surfaces. *ACS Nano* **2011**, *5* (2), 1360−1365.
(70) Payer, D.; Comisso, A.; Dmitriev, A.; Strunskus, T.; Lin, N.; Woll, C.; Devita, A.; Barth, J. V.; Kern, K. Ionic hydrogen bonds controlling two-dimensional supramolecular systems at a metal surface. *Chemistry* **2007**, *13* (14), 3900−6.
(71) Bradeanu, I. L.; Kosugi, N.; Flesch, R.; Rühl, E. Site-dependent spectral shifts in core-to-π^* excitations of pyridine clusters. *J. Phys. Chem. A* **2008**, *112* (39), 9192−9199.
(72) Bradeanu, I. L.; Flesch, R.; Kosugi, N.; Pavlychev, A. A.; Rühl, E. C 1s $\rightarrow$ π^* excitation in variable size benzene clusters. *Phys. Chem. Chem. Phys.* **2006**, *8* (16), 1906−1913.